ADVANCED ENERGY MATERIALS
www.advenergymat.de

In Situ Probing and Synthetic Control of Cationic Ordering in Ni-Rich Layered Oxide Cathodes

Jianqing Zhao, Wei Zhang, Ashfia Huq, Scott T. Misture, Boliang Zhang, Shengmin Guo, Lijun Wu, Yimei Zhu, Zonghai Chen, Khalil Amine, Feng Pan, Jianming Bai, and Feng Wang**

Ni-rich layered oxides ($LiNi_{1-x}M_xO_2$; M = Co, Mn, ...) are appealing alternatives to conventional $LiCoO_2$ as cathodes in Li-ion batteries for automobile and other large-scale applications due to their high theoretical capacity and low cost. However, preparing stoichiometric $LiNi_{1-x}M_xO_2$ with ordered layer structure and high reversible capacity, has proven difficult due to cation mixing in octahedral sites. Herein, in situ studies of synthesis reactions and the associated structural ordering in preparing $LiNiO_2$ and the Co-substituted variant, $LiNi_{0.8}Co_{0.2}O_2$, are made, to gain insights into synthetic control of the structure and electrochemical properties of Ni-rich layered oxides. Results from this study indicate a direct transformation of the intermediate from the rock salt structure into hexagonal phase, and during the process, Co substitution facilities the nucleation of a Co-rich layered phase at low temperatures and subsequent growth and stabilization of solid solution Li(Ni, Co)O_2 upon further heat treatment. Optimal conditions are identified from the in situ studies and utilized to obtain stoichiometric $LiNi_{0.8}Co_{0.2}O_2$ that exhibits high capacity (up to 200 mA h g^{-1}) with excellent retention. The findings shed light on designing high performance Ni-rich layered oxide cathodes through synthetic control of the structural ordering in the materials.

1. Introduction

Among the efforts to develop high-energy cathode materials for lithium-ion batteries, adding a second or even third cation to form solid solutions has been identified as an effective strategy for tailoring the structure and electrochemical properties of the electrodes.[1] One notable example is the NCM transition metal oxides (i.e., Li–Ni–Co(Mn)–O), the subject of intense investigation in the last decade.[2] Nevertheless, the study of this system is still far from complete due to the richness of the phases in the temperature-composition space and the complexity of the synthesis reactions. In addition to those known single phases (layered or spinel), there are a large number of composite phases and even new phases at the phase boundaries.[1a] Among the NCM phases, Ni-rich layered oxides $LiNi_{1-x}M_xO_2$ (M = Co, Mn, ...; $x \leq 0.4$) are particularly interesting for the high capacity (>200 mA h g^{-1}) and

Dr. J. Zhao, Dr. W. Zhang, Dr. F. Wang
Sustainable Energy Technologies Department
Brookhaven National Laboratory
Upton, NY 11973, USA
E-mail: fwang@bnl.gov
Prof. J. Zhao
School of Energy
College of Physics
Optoelectronics & Energy
Collaborative Innovation Center of
Suzhou Nano Science and Technology
Soochow University
Suzhou 215006, P. R. China
Dr. A. Huq
Chemical and Engineering Materials Division
Oak Ridge National Laboratory
Oak Ridge, TN 37831, USA
Prof. S. T. Misture
Kazuo Inamori School of Engineering
Alfred University
Alfred, NY 14802, USA

DOI: 10.1002/aenm.201601266

B. Zhang, Prof. S. Guo
Department of Mechanical & Industrial Engineering
Louisiana State University
Baton Rouge, LA 70803, USA
Dr. L. Wu, Dr. Y. Zhu
Condensed Matter Physics and
Materials Science Department
Brookhaven National Laboratory
Upton, NY 11973, USA
Dr. Z. Chen, Dr. K. Amine
Chemical Sciences and Engineering Division
Argonne National Laboratory
Argonne, IL 60439, USA
Prof. F. Pan
School of Advanced Materials
Peking University Shenzhen Graduate School
Shenzhen, Guangdong 518055, P. R. China
Dr. J. Bai
National Synchrotron Light Source II
Brookhaven National Laboratory
Upton, NY 11973, USA
E-mail: jmbai@bnl.gov

low cost. However, synthesis of stoichiometric Ni-rich layered oxides has been recognized as a great challenge attributed to cationic disordering (namely mixing of Li^+ with transition metal ions in octahedral sites).[3]

In $LiNi_{1-x}M_xO_2$, Ni^{2+} (with an electronic configuration of $t^6_{2g}e_g^2$) coexists with Ni^{3+} ($t^6_{2g}e_g^1$), and due to the similar ionic radii of the Li^+ (0.76 Å) and Ni^{2+} (0.69 Å) cation, Li^+/Ni^{2+} mixing takes place, i.e., partial occupancy of Ni^{2+} at 3b sites (in the Li^+ layers).[3a,i,4] Such structural disordering is considered the crucial issue accounting for the reduced capacity, poor cycling stability, and limited rate capability of Ni-rich layered cathode materials,[5] and much effort has been given to alleviate some of those problems through cationic substitution.[3i,6] For instance, Co^{3+} and/or Al^{3+} incorporation is known for stabilizing the layered structure and minimizing cation mixing in $LiNi_{1-x-y}Co_xAl_yO_2$, but sacrifices capacity; in addition, thermal stability remains the main limit to its commercial application.[1b] Adding Mn^{4+} has been shown effective in improving the thermal stability, but may aggravate the Li^+/Ni^{2+} cationic disordering because equivalent amounts of Ni^{2+} ions are introduced for charge compensation.[7] So far, despite many reports on cationic substitution for improving the ordering of layered structure, how such substitutions impact the cationic ordering in $LiNi_{1-x}M_xO_2$ during synthesis, and the eventual electrochemical properties, remains largely unknown.[8] One representative is $LiNi_{0.8}Co_{0.2}O_2$, of which there are varying and even conflicting reports of electrochemical performance despite the same stoichiometry, demonstrating the importance of synthetic control over structure and material properties.[9] However, synthesis reaction is complex, making preparation of electrode materials of desired phases and properties no easy task, and obtaining stoichiometric layered oxides $LiNi_{1-x}M_xO_2$ is even more challenging due to the high sensitivity of cationic ordering to the synthetic conditions such as heating temperature, duration time, and environment.[10] The recent studies showed that heating under high-oxidation environment (i.e., with O_2 flow) may help to achieve high structural ordering during synthesis of Ni-rich layered oxides.[10b,11]

Co substitution has been commonly used to obtain Li(Ni,Co)O_2 solid solution, wherein much improved structural ordering (compared to $LiNiO_2$) has been reported and attributed to the preferential electronic configurations Co^{3+} ions ($t^6_{2g}e_g^0$),[12] which has a similar ionic radius to Ni^{3+}, but much smaller than that of Li^+.[13] In order to better understand the effect of Co-substitution on the cationic ordering during synthesis, temperature-resolved in situ X-ray diffraction (XRD) measurements, combined with quantitative structure analysis, were performed to track the structural evolution during solid-state synthesis of $LiNiO_2$ and Co-substitute variant, $LiNi_{0.8}Co_{0.2}O_2$ using same synthesis conditions (both under O_2 flow and in the air; see details in the Experimental Section). Complementary thermogravimetric analysis (TGA), along with synchrotron XRD, neutron powder diffraction (NPD), and transmission electron microscopy (TEM), electron energy-loss spectroscopy (EELS) measurements, was made to identify chemical reactions during heating and the structural ordering of the synthesized materials. The results from this investigation indicated that Co tends to form a solid solution with Ni within the rock-salt, and so facilitates initial nucleation of a Co-rich layered phase at low temperatures, and also plays an important role in the subsequent growth and stabilization of layered structure by suppressing lithium loss during heat treatment at high temperatures. By using optimal conditions (determined in situ), stoichiometric $LiNi_{0.8}Co_{0.2}O_2$ was synthesized, and due to the low cationic disordering (below 2%), the electrodes made from the material exhibit high capacity, up to 200 mA h g^{-1} , and excellent cycling stability. The findings shed light on designing high performance Ni-rich layered oxide cathodes through synthetic control of the structural ordering in the materials.

2. Results

2.1. Synthesis Reactions Studied via TGA and In Situ XRD

TGA and XRD analysis was made to the structural evolution of precursors and intermediates during synthesis of $LiNiO_2$ and $LiNi_{0.8}Co_{0.2}O_2$; the main results were given in the Supporting Information (Figure S1a,d). Clearly, when heated in the air the TGA and differential thermal analysis (DTA) response of the precursors for $LiNi_{0.8}Co_{0.2}O_2$ is different than that under highly oxidizing environment, e.g., under O_2 flow (Figure S1b,c, Supporting Information). The difference is better seen in a close view at the temperature range of 700–950 °C (insets of Figure S1b,c, Supporting Information): a continuous mass loss (indicated by sloppy profile in the TGA curve) occurs in the air, in contrast to the flat plateau under O_2 flow—indicating the probability of stabilizing a layered phase with subtle structural changes and weight loss. Nevertheless, even subjected to the same heating process in the O_2, the precursors for synthesizing $LiNiO_2$ and $LiNi_{0.8}Co_{0.2}O_2$ underwent different phase/structure evolution, as indicated by the TGA/DTA response; specifically, an extensively long slope is shown in the TGA curve, along with an apparent endothermic reaction in DTA for the former, implying complex structural re-arrangements and/or phase transitions without Co-substitution (as further confirmed by in situ XRD measurements). In addition, Figure S1d of the Supporting Information shows XRD patterns of the intermediate phases prepared at 400 °C for 5 h in O_2 flow and in the air. As shown in the selected enlarged portion I, the strong (003) peak in the intermediate for synthesizing $LiNi_{0.8}Co_{0.2}O_2$ under O_2 flow, with much higher intensity than that in the air, indicates the importance of high oxidation sintering environment on structural ordering in Ni-rich layered oxides. On the other hand, even under O_2 flow the characteristic peak (003) of the layered structure is absent in the pure $LiNiO_2$, implying that Co substitution facilitates the formation of layered structure at low heating temperature. These results from combined TGA/DTA, XRD analysis suggest that both O_2 flow and Co substitution are crucial to obtaining highly ordered layer structure in Ni-rich oxides.

Figure 1a,b shows temperature-resolved XRD patterns recorded during synthesis of $LiNiO_2$ and $LiNi_{0.8}Co_{0.2}O_2$, subjected to heat treatment at temperatures ranging from 300 to 1000 °C under pure O_2 environment. The XRD was recorded with one pattern per 100 °C at temperatures below 600 °C and then every 25 °C at temperatures above 650 °C by considering that the layered structure of Ni-rich oxides is highly sensitive

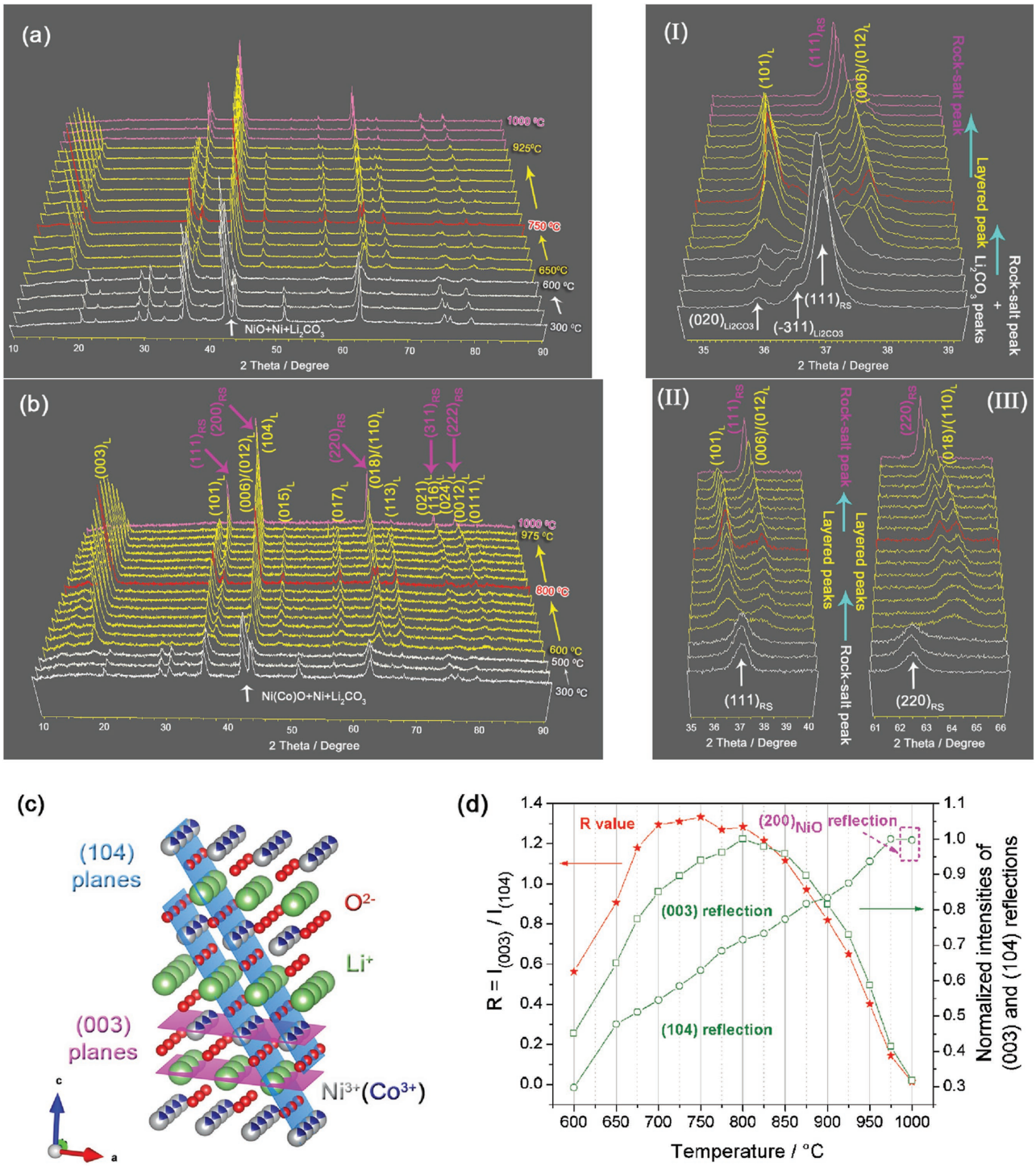

Figure 1. In situ tracking structural evolution of the intermediates during solid-state synthesis of Ni-rich oxides in O_2 flow. a,b) In situ XRD patterns recorded during synthesis of $LiNiO_2$ and $LiNi_{0.8}Co_{0.2}O_2$, respectively, along with enlarged 2θ portions, (I) between 35° and 39° from (a), (II, III) between 35°–40° and 61°–66° from (b), indicating a direct transition from the initial rock salt into the layered phase (as illustrated). c) Illustration of the atomic configure and reflection planes of (104) and (003) in the layered structure, indicating the high sensitivity of the (003) reflection to the cationic ordering (i.e., occupancies of Li, Ni, and Co ions), in contrast to the independence of (104) on the ordering. d) Evolution of the intensity of (003) and (104) reflections during synthesis of $LiNi_{0.8}Co_{0.2}O_2$ (green circles and squares, respectively, with lines as a guide to the eye), and the ratio of the two, $R = I_{(003)}/I_{(104)}$ (red stars with the line as a guide to the eye); the values were extracted from in situ XRD patterns in (b).

to the temperature.[10a] The in situ XRD observation during the synthesis of pure $LiNiO_2$ (Figure 1a) is overall consistent with the results from TGA/DTA measurements (Figure S1b,c, Supporting Information), indicating a three-stage process, but with detailed information about structural evolution (better viewed in the enlarged 2θ portion I between 35° and 39°). In

the initial stage, the precursor materials undergo interaction between different components and decomposition, leading to rock-salt NiO, Li_2CO_3 at low temperatures and subsequent formation of a Li-deficient layered phase at about 650 °C. At 300 °C, in addition to NiO and Li_2CO_3, an unexpected metallic Ni^0 phase was detected by XRD, immediately after decomposition of acetate-based precursor (Figure 1a). The intriguing existence of Ni^0 metal instead of the reported Ni_2O_3 phase may be attributed to the carbothermal reduction effects from the decomposition of the acetate-based precursors,[14,15] which is successively oxidized to NiO at about 500 °C. An enlarged depiction between 35° and 39° indicates Li-deficient characteristics for such an initially formed layered phase, because the $(006)/(012)_L$ doublet, characteristic of the layered structure, is mostly overlapped into a single peak as shown in 2θ portion I at 650 °C.[16]

In the subsequent, second stage above 650 °C, structural evolution of the as-formed layered phase becomes subtle and complex, involving the competition between structural ordering and degradation as a result of simultaneous incorporation of lithium from the precursor source, and loss of lithium from the lattice structure. The structural ordering of layered $LiNiO_2$ is demonstrated by peak intensity evolution of the (003) reflection, or the ratio of the integrated intensity $R = I(003)/I(104)$ since the reflection from (104) planes is independent of the ordering as illustrated in Figure 1c. In addition, the ordering also manifests with the peak splitting of $(006)/(012)_L$ pair (as presented in 2θ portion I).[16] The best ordering of the layered structure is formed at about 750 °C with *R-3m* symmetry (as highlighted in red in Figure 1a), according to the intensity profile of (003) reflection or the ratio $R = I(003)/I(104)$ (Figure S2, Supporting Information), and the peak splitting of $(006)/(012)_L$ doublet (2θ portion I).

In the 3rd stage, during further heat treatment at high temperatures (above 750 °C), structural degradation occurs (resulting from Li and O loss, as to be discussed below), and at temperatures above 925 °C the layered $LiNiO_2$ suffers from a gradual phase change back to a NiO-like structure instead of a rapid decomposition process. Such a phase change is indicated by the disappearance of the $(003)_L$ reflection (Figure 1a), along with merging of the $(006)/(012)_L$ pair and loss of the $(101)_L$ peak (2θ portion I). In summary, the synthesis process of $LiNiO_2$ oxide involves complex structure evolution as follows: an initial Li-deficient layered phase is formed by consuming precursor materials at low temperatures; subsequently, the ordering of layered structure occurs with further lithiation, as well as simultaneous degradation of the as-formed layered phase, eventually leading to a phase change back to the rock salt at high temperatures.

In Figure 1b, the in situ XRD patterns recorded during synthesis of $LiNi_{0.8}Co_{0.2}O_2$ show a similar trend of phase evolution as that during synthesis of $LiNiO_2$ (Figure 1a); nevertheless, there is subtle but distinguishable difference, indicating a different cationic ordering process toward forming the layered structure. During the initial stage of precursor decomposition, no separated rock-salt phases of NiO, or CoO (or spinel Co_2O_3) were found; but instead a solid solution Ni(Co)O was formed (Figure 1b and Figure S1, Supporting Information) at low temperatures. Interestingly, a low-temperature layered phase, with lattice parameter close to that of $LiCoO_2$, was found at a temperature as low as 500 °C. It is likely that a Co-rich layered phase has formed as a result of local segregation of Li^+ and Co^{3+} in octahedral sites since the two have large difference in ionic radius (0.76 Å vs 0.55 Å). The nucleation of this layered phase appears to be beneficial to initializing the Li-deficient layered phase, at a temperature of about 600 °C, lower than that during synthesis of $LiNiO_2$ (Figure 1a). Furthermore, the appearance of the $(003)_L$ reflection (related to the initial Li-deficient layered phase) can even be detected at a temperature as low as 400 °C during ex situ synthesis (Figure S1d; with 5 h of heat treatment); in contrast, no $(003)_L$ peak is found in the XRD pattern recorded at 400 °C during synthesis of pure $LiNiO_2$ at such a low heating temperature.

As the temperature is further elevated, the peak splitting of the $(006)/(012)_L$ and $(018)/(110)_L$ doublets (2θ portion II and III from Figure 1b) becomes larger, and correspondingly the intensity of the (003) reflection increases, revealing the gradual ordering of the layered structure, eventually resulting in an optimal layered $LiNi_{0.8}Co_{0.2}O_2$ at about 800 °C (Figure 1d). The structural ordering of Ni-rich layered oxides can also be determined by the ratio, $R = I(003)/I(104)$. The R value was about 0.55 at 600 °C and then quickly increased to 0.92 by 650 °C (Figure 1d; much higher than the value for $LiNiO_2$ as in Figure S2, Supporting Information), which clearly indicates the importance of Co substitution for the nucleation and growth of the Li-deficient layered phase at low temperatures. The maximum value of the ratio R is 1.29 in $LiNi_{0.8}Co_{0.2}O_2$, much higher than the value 0.92 found for $LiNiO_2$ (Figure S2, Supporting Information), indicating a significant enhancement of structural ordering of the layered Ni-rich oxide due to Co substitution. In comparison to the rapid degradation of $LiNiO_2$ at high temperatures, $LiNi_{0.8}Co_{0.2}O_2$ can retain the layered structure up to 950 °C, without transition to the rock-salt phase until 975 °C (Figure 1b), showing the remarkable enhancement of thermal stability by Co substitution. The presence of Co appears to be crucial to stabilizing the layered structure against lithium and oxygen loss.[12]

2.2. Evolution of Structural Ordering in Layered Oxides

Complex phase transformation and structural ordering are involved during synthesis of layered $LiNi_{0.8}Co_{0.2}O_2$ (Figure 1b). In order to obtain details about synthesis process, Rietveld refinements were made to individual in situ XRD patterns acquired at intermediate and high temperatures (above 600 °C). The main results are presented in **Figure 2** and Tables S1 and S2 of the Supporting Information. Since the scattering of X-rays by Ni and Co is hardly distinguishable, we fix the molar ratio of Co over Ni to 0.25 by assuming that all Co cations can only occupy 3a sites, which is roughly consistent with the results from neutron measurements (to be presented below; Table S3, Supporting Information). A Li-deficient layered phase, which was modeled as $Li_{1-x}Ni^{2+}_x(Ni^{3+}_{0.8-1.2x}Ni^{2+}_xCo_{0.2(1+x)})O_2$,[4a] starts to form at 600 °C, with residual Li_2CO_3 and NiO phases (Figure 2a; Table S2, Supporting Information). Figure 2b shows a parabolic evolution of the Li^+ occupancy at 3b sites (or Li sites) in the Li-deficient layered phase, which matches well with the intensity change of the $(003)_L$ reflection (Figure 1d). The Li

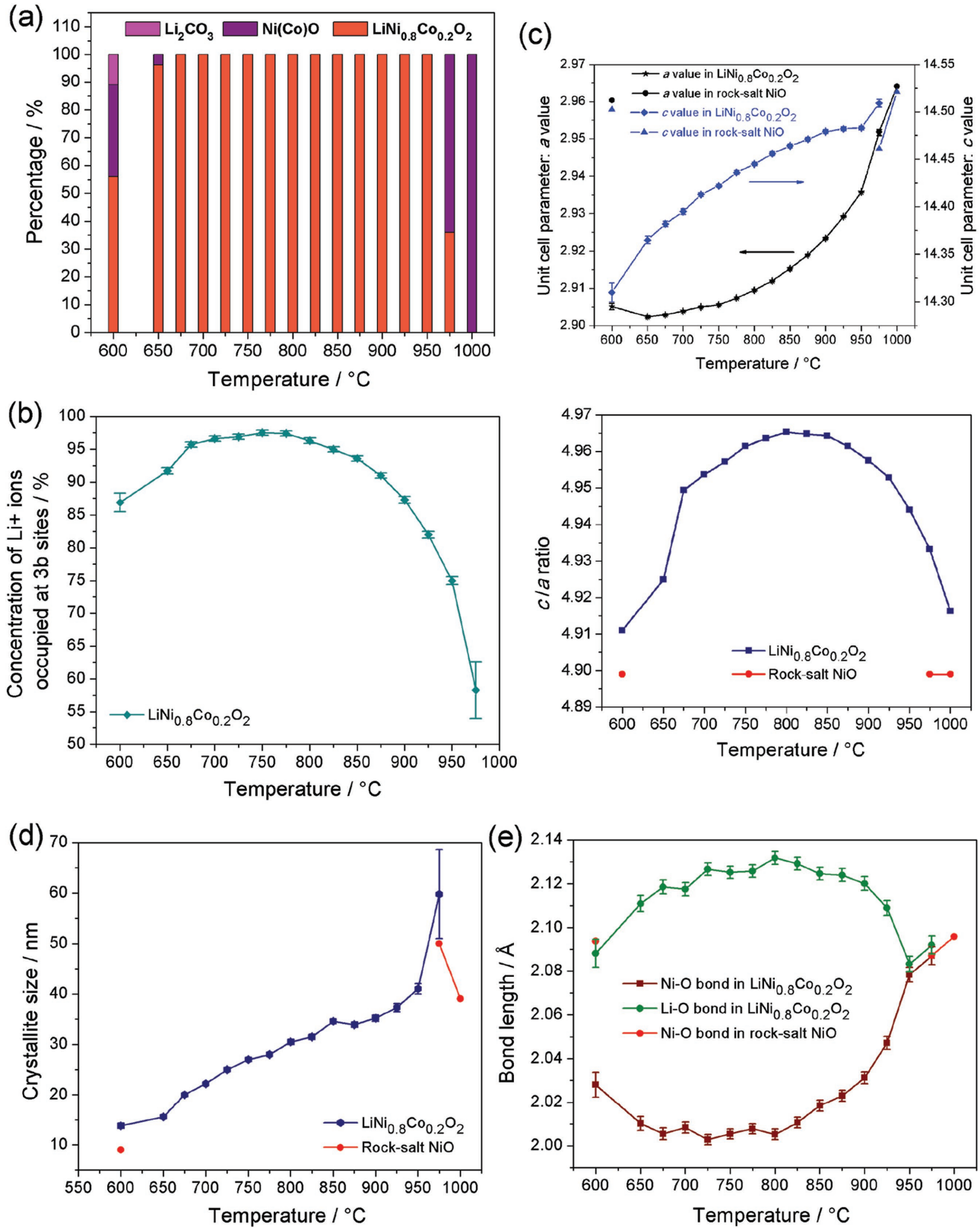

Figure 2. Evolution of the involved phases, and structural ordering of $LiNi_{0.8}Co_{0.2}O_2$ with temperature during heat treatment in the O_2 flow. a) Concentration of the involved phases (Ni(Co)O, Li_2CO_3, and $LiNi_{0.8}Co_{0.2}O_2$). b) Li^+ occupancy at 3b sites (Li sites). c) Unit cell parameters *a*, *c* and the ratio *c*/*a* . d) Crystallite size. e) Ni–O and Li–O bond lengths. Data from NiO phase were also included for comparison (red dots). Lines were used as a guide to the eye.

concentration in the layered phase was 86.8% at 600 °C, and then continuously increased during further heat treatment, going up to 97.5% at 750 °C, as a result of continuous lithiation. Although the lithium source Li_2CO_3 was not detected by in situ XRD at temperatures above 600 °C (Figure 1b), Li_2CO_3 may still exist because the neutron diffraction pattern (NDP) revealed residual Li_2CO_3 in the $LiNi_{0.8}Co_{0.2}O_2$ sample calcinated at 800 °C for 5 min (Figure S3, Supporting Information). Further heat treatment at higher temperatures (above 800 °C) leads to Li/O loss, as indicated by the mass loss in the TGA curve (Figure S1b, Supporting Information),[11b] and as a result the Li occupancy at 3b starts to drop (Figure 2b).

The ratio of the cell parameters, c over a, i.e., c/a, has been demonstrated to correlate with the degree of ordering in the layered structure since a cubic cell can be represented with a hexagonal unit cell with $c/a = 4.899$. The c/a ratio deviates from the value for cubic cell during the lithiation process: the larger the value of c/a is, the better ordering of the layered structure. In Figure 2c, a, c, and relative c/a values as a function of heating temperature are provided, indicating the best-ordered layered structure at about 800 °C. The metal-oxygen bond length in an octahedral site is an indication of the oxidation state and the occupation ratio of the metals co-occupying the site. The average bond length at 3b site, co-occupied by Li^+ ($r = 0.76$ Å) and Ni^{2+} ($r = 0.69$ Å) is longer than that at 3a site, populated with Ni^{3+} ($r = 0.56$ Å), Co^{3+} ($r = 0.55$ Å), and Ni^{2+}, as shown in Figure 2e. As the Li^+ occupancy at the 3b site increases, the bond length at the 3b site becomes longer while the length at the 3a site becomes inversely shorter, as there are less Ni^{+2} in the transition metal layer. Both the longest M–O bond length at 3b sites (mostly Li–O) and the shortest Ni/Co–O bond length at 3a sites are found at 800 °C. The slight difference of the optimal temperatures based on different characteristics can be attributed to the uncertainties of different refinement parameters, especially those of the Li content determined by Rietveld refinements. Since the optimal temperature is a result of competition between the lithiation and the lithium/oxygen loss in the layered structure, the observation of higher optimal temperature in $LiNi_{0.8}Co_{0.2}O_2$, compared to that of $LiNiO_2$ (750 °C), signifies the stabilization effect of the Co substitution. As the temperature goes beyond the optimal temperature, the bond lengths at the 3a and 3b sites start moving in opposite directions. At 950 °C, the metal-oxygen bond lengths at the two sites are virtually the same, and the rock salt phase is observed at 975 °C. In addition, the refinement results in Figure 2d also show a gradual increase of crystallite size in $LiNi_{0.8}Co_{0.2}O_2$ materials, indicating crystal growth during heat treatment at high temperatures, which is consistent with the gradual increase of the peak intensity of (104) reflection (Figure 1d). The sudden particle growth above 950 °C is probably a result of the phase change from the Ni-rich layered oxide to rock-salt NiO at such high temperatures.

In summary, the results from in situ studies along with quantitative structure analysis indicate a direct phase transition from rock salt to the layered phase both in $LiNiO_2$ and $LiNi_{0.8}Co_{0.2}O_2$, followed by improving the cationic ordering of the layered structure with further lithiation. Significant impact of cobalt substitution to structural ordering in layered Ni-rich oxides was observed, as follows: first, the substituted Co can facilitate the initial nucleation of a layered phase at 600 °C or lower; second, the Co incorporation reduces cation mixing and degree of cation disordering.[17] Finally, Co substitution considerably enhances structural stability of Ni-rich layered oxides, resulting in retention of the layered structure at higher temperatures. Based on the results from in situ XRD studies, we conclude that the best ordered layered structure should be formed at around 775–800 °C, corresponding to a formula of $(Li_{0.97}Ni_{0.03})_{3b}(Ni_{0.764}Co_{0.206})_{3a}O_2$.

2.3. Structural Properties of the Synthesized Materials

$LiNi_{0.8}Co_{0.2}O_2$ powder was synthesized under the optimal condition (at 800 °C in O_2 flow for 5 h, labeled as $LiNi_{0.8}Co_{0.2}O_2$-800-O_2-5h), as determined from in situ XRD studies, and its structure was examined using high resolution synchrotron XRD and NPD, along with Rietveld refinement. The main results were presented in **Figure 3** and Tables S3 and S4 of

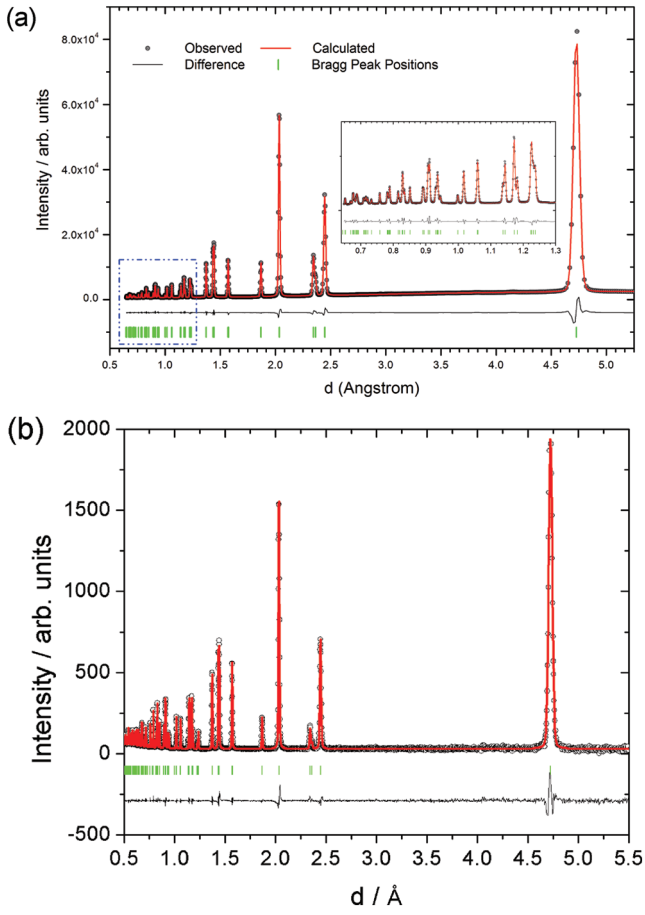

Figure 3. Structural analysis of $LiNi_{0.8}Co_{0.2}O_2$ powder synthesized under optimized conditions (at 800 °C in O_2 flow for 5 h). a) Synchrotron X-ray diffraction (XRD), b) neutron powder diffraction (NPD) patterns, in comparison to the calculated patterns by Rietveld refinement. In the plots, black dots are used for the observed data, red lines for calculated data, green bars for Bragg positions, and gray lines for the difference between the observed and calculated data (Rwp = 4.49% and 5.04% from the refinement of XRD and NPD patterns, respectively).

the Supporting Information. With long enough time of heat treatment, the sample $LiNi_{0.8}Co_{0.2}O_2$-800-O_2-5h shows high cationic ordering (with 98.0% Li occupancy at 3b sites), with a value slightly larger than that obtained from the in situ data (97.5%). It should be noted that the in situ XRD patterns were taken with a holding time of 1 h that may not be long enough for the system to reach the equilibrium state. This result shows high cationic ordering, with desired occupation of Li ions and Ni/Co cation within the lithium and transition metal layers, respectively, in contrast to the high disordering in the synthesized $LiNiO_2$ under optimal condition (at 750 °C in O_2 flow for 5 h), of about 96.5% (Table S3, Supporting Information). The results from NPD measurement (Table S4, Supporting Information) are overall consistent with that from synchrotron XRD, indicating the Li occupancy of 98.5% at 3b sites, much higher than that of the sample optimized in air, 93.0% (at 900 °C in the air for 20 h—the optimal conditions determined by many trials; Figure S4, Supporting Information). The occupancy of Ni and Co at 3a sites was also obtained from the refinement of the NPD data, being 3.76 for the Ni/Co ration in the $LiNi_{0.8}Co_{0.2}O_2$-800-O_2-5h sample (Table S3, Supporting Information), lower than the theoretical value of 4. Such difference becomes more significant for $LiNi_{0.8}Co_{0.2}O_2$-900-A-20h with a Ni/Co ratio of 3.40 (due to the disordering, with more Ni on 3b sites). Hence, the stabilization and enhanced ordering of layered structure for Ni-rich oxides from Co substitution can be highly expected due to the relatively stable occupancy of Co cation at 3a sites, and high oxidation heat treatment environment is desirable for the synthesis of Ni-rich layered oxides.

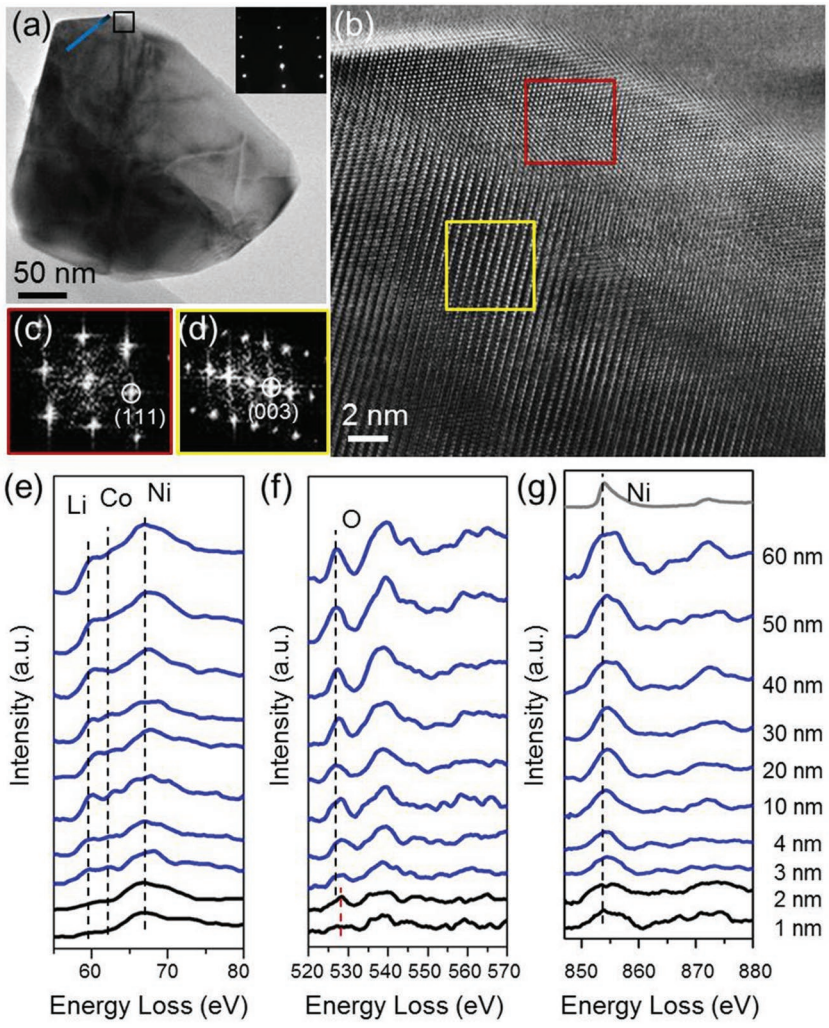

Figure 4. Local structural/chemical analysis of individual $LiNi_{0.8}Co_{0.2}O_2$ particles. a) A bright-field TEM image showing the typical morphology of $LiNi_{0.8}Co_{0.2}O_2$ particles, and corresponding selected area electron diffraction pattern (recorded from the whole particle; inset) indicating the single-crystalline layered structure of the particle. b) A HRTEM image obtained from the local region marked by black box in (a). c,d) Fast Fourier transformation (FFT) patterns obtained from two local areas marked by red and yellow boxes in (b), indicating the different structure at surface (rock-salt) than that of the bulk (layered). e–g) EELS spectra of Li, O K-edges, Co, Ni M-edges, and Ni L-edge (as labeled) recorded along the blue line in (a). The spectra generated from the surface region were drawn in black color, while the ones from the bulk region in blue color. The reference spectra of Ni–L edge from NiO (in gray) was given in (g; top).

Local structural characterization using scanning TEM (STEM), EELS, and electron diffraction was performed to individual particles of the $LiNi_{0.8}Co_{0.2}O_2$ and $LiNiO_2$ (see the main results in **Figure 4** and Figure S5, Supporting Information). Here, the calculated crystallite size of $LiNi_{0.8}Co_{0.2}O_2$ is much smaller than that shown in the TEM images, which may be attributed to the nonuniform size distribution and polycrystal structure of the particles. As shown by the electron diffraction patterns in the inset of Figure 4a and Figure S5a of the Supporting Information, both samples possess layered structure, being consistent with synchrotron XRD and NPD results (Figure 3a and Figure S6, Supporting Information). However, the rock salt structure can be captured for these two samples at the surface. The high-resolution TEM image recorded in the near-surface region of $LiNi_{0.8}Co_{0.2}O_2$-800-O_2-5h (Figure 4b), indicates the formation of NiO-type rock salt.[18] This was also shown by the difference of fast Fourier transform (FFT) pattern (Figure 4c), compared to that recorded from the bulk region (with a layered structure; Figure 4d). The surface rock-salt phase is more phenomenal in the $LiNiO_2$-750-O_2-5h sample (Figure S5c,d, Supporting Information). EELS spectra were also collected from these two samples to reveal the lithium distribution and valence states of transition metal cation (Figure 4e–g and Figure S5e–g). The presence of a NiO-type structure at surface regions of both samples can be confirmed by the higher energy of the pre-peak of O K-edge (indicated by the red dashed lines in Figure 4f and Figure S5f).[18] The Li K-edge of $LiNi_{0.8}Co_{0.2}O_2$-800-O_2-5h shows the lithium concentration gradient through the whole linear scan from the surface to the bulk in Figure 4e, and the nearly-constant peak

positions of Ni $L_{2,3}$ edge spectra show the valence of Ni roughly remains trivalent state from surface into the bulk (with small concentration of Ni^{2+}; Figure 4e,g). In contrast, the lithium signal only appears at the position away from the surface, by about 2 nm, in pure $LiNiO_2$-750-O_2-5h (Figure S5e, Supporting Information), and the valence state of Ni ions changes from divalent to trivalent by around 20 nm (Figure S5g, Supporting Information). Such differences in EELS results can be attributed to the presence of Co (to the outmost surface), which helps to stabilize Ni^{3+} ions and preventing from lithium and oxygen loss at the surface of layered $LiNi_{0.8}Co_{0.2}O_2$-800-O_2-5h. As reported in the literatures,[19] the diffusion energy barrier of Ni cations in the lithium layer is even smaller than that of Li^+ ions, and so Ni segregation may occur at the particle surface, and thus accelerates the lithium and oxygen loss during the synthesis. Since Co-substitution can effectively prevent the reduction of Ni^{3+} to Ni^{2+} and subsequent Ni^{2+} migration, so the lithium and oxygen loss in $LiNi_{0.8}Co_{0.2}O_2$ may be much reduced as compared with pure $LiNiO_2$.

2.4. Electrochemical Properties of the Synthesized Materials

Figure 5 shows the electrochemical performance of the electrodes made from the samples of $LiNiO_2$-750-O_2-5h, $LiNi_{0.8}Co_{0.2}O_2$-800-O_2-5h as well as the $LiNi_{0.8}Co_{0.2}O_2$ synthesized in the air at an optimal temperature of 900 °C for 20 h (marked as $LiNi_{0.8}Co_{0.2}O_2$-900-A-20h; Figure S4, Supporting Information). In addition to the charge/discharge curves at different cycles, corresponding differential capacity (dQ/dV) profiles were also provided. Here, the differential capacity versus voltage was used to demonstrate a more realistic performance of cathode materials subjected to the galvanostatic cycling, which is different from the cyclic voltammetry (CV) response that only describes a quasi-equilibrium state of electrodes with respect to the varying voltage. The sample $LiNiO_2$-750-O_2-5h delivers initial charge and discharge capacities of 267.2 and 221.2 mA h g^{-1} at a rate of 0.1 C (Figure 5a) through various phase transitions among three hexagonal phases (H1, H2, and H3) and one monoclinic phase (M) during lithium deintercalation and intercalation (Figure 5b).[20,21] As shown in Figure 5c, the $LiNi_{0.8}Co_{0.2}O_2$-800-O_2-5h exhibits relatively lower charge capacity, 197.8 mA h g^{-1}. Since the "t_{2g}" band of low-spin Co^{3+} is completely filled (t^6_{2g}) and its energy level is lower than that of Ni^{2+}/Ni^{3+} and Ni^{3+}/Ni^{4+} couples, the oxidation of Co^{3+}/Co^{4+} is difficult to reach at a upper cutoff voltage 4.3 V versus Li/Li^+, leading to reduced capacity in $LiNi_{0.8}Co_{0.2}O_2$ (compared to the pristine $LiNiO_2$).[21] Furthermore, it is noticeable that the charge/discharge and associated dQ/dV profiles (Figure 5d) of $LiNi_{0.8}Co_{0.2}O_2$-800-O_2-5h cathode are distinct from that of $LiNiO_2$-750-O_2-5h (Figure 5a,b), indicating the different lithium deintercalation and intercalation processes. As aforementioned, there is no redox reactions and capacity contribution from the substituted Co^{3+} cation within the voltage range of 2.7–4.3 V versus Li/Li^+. All peaks in dQ/dV features in Figure 5d and anodic and cathodic peaks in CV curves (in the inset) are related to Ni^{3+}/Ni^{4+} redox. The CV profiles of $LiNi_{0.8}Co_{0.2}O_2$-800-O_2-5h are identical to that reported in the literature,[22] revealing only one phase transition from H1 to H2 occurred between 4.1 and 4.3 V during the lithium de/intercalation process. The predominant anodic peaks around 3.79 V with a weak shoulder at 4.03 V is attributed to the oxidation of Ni^{3+}/Ni^{4+} redox within the original hexagonal H1 structure of $LiNi_{0.8}Co_{0.2}O_2$, along with two corresponding cathodic peaks at 3.63 and 3.92 V, respectively. The electrochemical performance demonstrate the effect of Co-substitution on restricting phase transitions for Ni-rich layered oxides, resulting in phenomenally enhanced cycling stability as shown in Figure 5f. When the $LiNi_{0.8}Co_{0.2}O_2$ electrode was cycled in an extended voltage range, between 2.7 and 4.6 V (see also charge/discharge profiles in Figure S7, Supporting Information), much higher capacity (above 200 mA h g^{-1}) was achieved. Such high reversible cycling capacity should have not been achieved in $LiNi_{0.8}Co_{0.2}O_2$ without optimizing synthesis conditions. As reported earlier, the low cation disordering, below 2%, was considered as the threshold for achieving desired good performance in the layered $LiNi_{1/3}Mn_{1/3}Co_{1/3}O_2$,[23] which may also be applicable to the $LiNi_{0.8}Co_{0.2}O_2$. As expected, low specific capacity and poor cycling performance were obtained in $LiNi_{0.8}Co_{0.2}O_2$-900-A-20h (Figure 5e) largely due to the structural disordering and more severe Li^+/Ni^{2+} cation mixing (Table S4, Supporting Information). As reported in the literature,[24] electrochemical performances of Ni-rich layered cathode materials are highly correlated to surface characteristics and particle size even with the similar bulk properties. In addition to the severe Ni^{2+}/Li^+ cation mixing in $LiNi_{0.8}Co_{0.2}O_2$ -900-A-20h, ≈7% (Table S4, Supporting Infromation), the thicker formation of rock-salt phase at the surface (of 10–15 nm) and large particle size (in micrometer range) should also account for its significantly lower capacity than that in $LiNi_{0.8}Co_{0.2}O_2$-800-O_2-5h (Figure 5d,f and Figure S8, Supporting Information).

3. Discussion

3.1. Mechanisms of Cationic Ordering in Ni-Rich Layered Oxides

Through in situ XRD measurements of the synthesis reactions of $LiNiO_2$ and the Co-substituted variant, $LiNi_{0.8}Co_{0.2}O_2$, this study revealed the evolution of cationic ordering in the intermediates during heat treatment, indicating that the synthesis processes of the two systems are similar overall, both involving direct phase transformations from rock salt to the layered structure and then back to the rock salt phase. A notable difference is that, during synthesis of $LiNi_{0.8}Co_{0.2}O_2$, Co-substitution promotes the nucleation of Co-rich layered phase at low temperatures, and subsequent growth and stabilization of the solid solution $Li(Ni, Co)O_2$ during further heat treatment at high temperatures. Such a direct transformation from rock-salt to the layered structure in Ni-rich oxides differs from that during synthesis of Co-based layered oxides, such as $LiCoO_2$, wherein an intermediate spinel $Li_2Co_2O_4$ was revealed.[25] Taken together, the results from in situ studies of the synthesis processes in these contrasting systems, namely, $LiNiO_2$, $LiNi_{0.8}Co_{0.2}O_2$, and $LiCoO_2$ (as in ref. [25]), suggest that the nature of the cation (i.e., ionic radius, size, valence state) plays a significant role in determining cationic ordering and phase transformation during

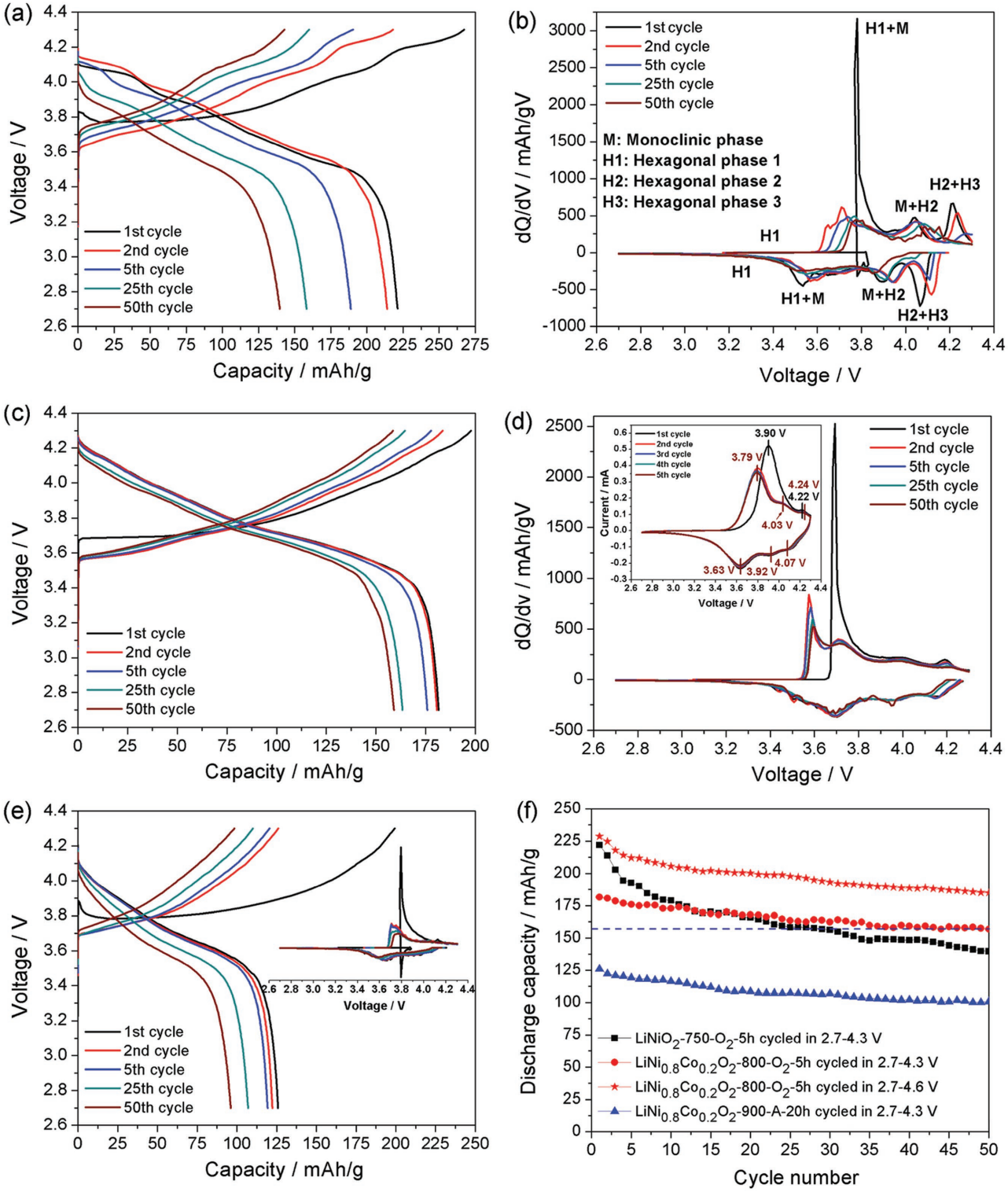

Figure 5. Electrochemical performance of $LiNiO_2$ and $LiNi_{0.8}Co_{0.2}O_2$ synthesized under different conditions. a,b) Voltage profiles of $LiNiO_2$ during charge/discharge at 0.1 *C* (calculated using 200 mA g^{-1} as nominal capacity), and corresponding differential capacity curves (sample: $LiNiO_2$-750-O_2-5h, synthesized in O_2, at 750 °C for 5 h). c,d) Voltage profiles of $LiNi_{0.8}Co_{0.2}O_2$ during charge/discharge at 0.1 *C*, and corresponding differential capacity curves (sample: $LiNi_{0.8}Co_{0.2}O_2$-800-O_2-5h, synthesized in O_2, at 800 °C for 5 h), along with the CV profiles (inset in (d)). e) Voltage profiles of $LiNi_{0.8}Co_{0.2}O_2$ during charge/discharge at 0.1 *C* (sample: $LiNi_{0.8}Co_{0.2}O_2$-900-A-20h, in the air, at 900 °C for 20 h), and corresponding differential capacity curves (inset). f) Cycling performance of the three samples at 0.1 *C* in the voltage range of 2.7–4.3 V, along with the performance of $LiNi_{0.8}Co_{0.2}O_2$-800-O_2-5h in the voltage range of 2.7–4.6 V, demonstrating achievable higher capacity in the extended voltage range.

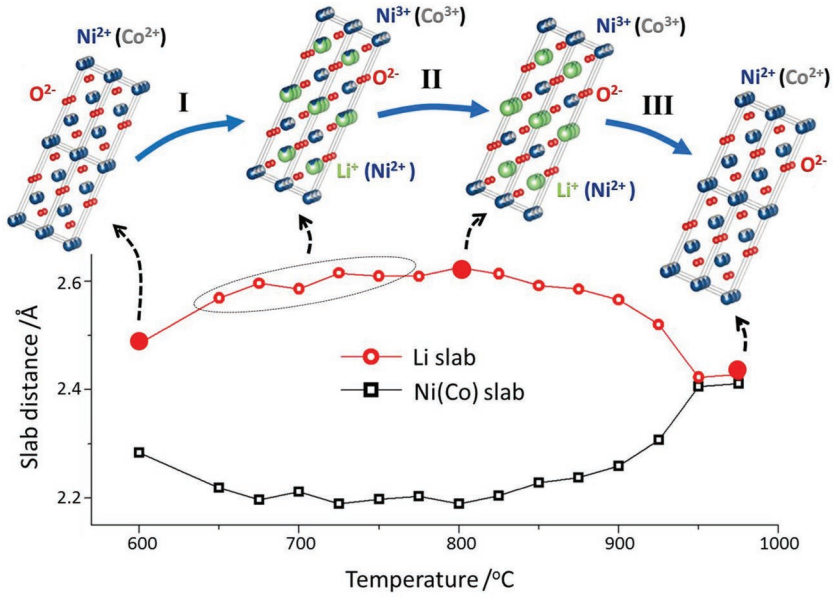

Figure 6. Schemtic illustration of the phase evolution, cationic ordering of the intermediates as a function of temperature (top), and the corresponding Li and Ni(Co) slab distances (bottom) during solid-state synthesis of layered oxides, exampled using $LiNi_{0.8}Co_{0.2}O_2$.

synthesis of layered oxides, as illustrated in **Figure 6** (top panel) and discussed immediately below.

In the early stage (Stage I), the transition from rock salt to the layered structure takes place at low temperatures, i.e., the initial lithiation of NiO to form Li-deficient layered phase ($Li_xNi_{2-x}O_{2-\delta}$). A 2D layered $Li_xNi_{1-x}O_{2-\delta}$ with *R-3m* symmetry can actually be alternatively considered as the ordered arrangement of Li^+ and Ni^{3+} cations along the [111] direction of the rock-salt lattice with face-center-cubic (FCC) characteristics (as shown in Figure 6; top panel).[11a,13] The long Ni–O bond length (or the large spacing of between O layers; Figure 2e), may allow Li^+ ions to diffuse into the Ni^{2+} layer in the NiO and randomly mix with Ni^{2+} without ordering (since the two have similar ionic radii), which may explain the direct transformation from rock salt to the layered phase, without going through the spinel phase (being observed during synthesis of Co-based layered oxides).[25] At current stage (with Li-deficient layered phase $Li_xNi_{2-x}O_{2-\delta}$ formed), there is significant amount Ni^{2+} highly mixed with Li^+ both in the 3a (TM sites) and 3b sites (Li sites), as suggested by the proposed model by Delmas et al.: $Li_{1-x}Ni^{2+}{}_x(Ni^{3+}{}_{0.8-1.2x}Ni^{2+}{}_xCo_{0.2(1+x)})O_2$.[4a] According to the refinement results in Figure 2 (for the case of $LiNi_{0.8}Co_{0.2}O_2$), there is a large portion of the NiO phase, ~35% at 600 °C (Figure 2a), and the Li–O bond is pretty much same as the Ni–O in the NiO phase (Figure 2e), which indicates the high mixing of Li^+/Ni^{2+} at low temperatures, with Ni^{2+} predominantly from NiO at the initial lithiation stage.

In the oxidizing atmosphere, the oxidization of Ni^{2+} into smaller Ni^{3+} ions leads to cation segregation, turning rock salt into a layered structure locally (as illustrated in Figure S9, Supporting Information). In other words, the lithiation of rock-salt NiO results in the formation of Ni^{3+} and subsequent alternative occupancies of Li^+ and Ni^{3+} within the FCC oxygen framework (Figure 6). With Co-substitution, the lithiation in $LiNi_{0.8}Co_{0.2}O_2$ proceeds through a transient $LiCoO_2$-like phase at low temperatures (as illustrated in Figure S9, Supporting Information)), which may play an important role in the subsequent growth and stabilization of solid solution Li(Ni, Co)O_2.

During further heat treatment at elevated temperatures (Stage II), more Ni^{2+} ions are oxidized into Ni^{3+}, leading to further Li^+/Ni^{3+} cationic segregation and ordering (Figure 6), as clearly shown by the gradual increase in Li^+ population at 3b sites and by changes in the bond length of Ni–O/Li–O (Figure 2e). However, heat treatment also leads to simultaneous Li loss from the layered structure, especially at high temperatures (750 °C and above), leading to degradation of the structural ordering (namely, migration of Ni^{2+} cation into the Li layer) and transformation back to rock salt in the near surface region. During high temperature treatment (Stage III), Li^+/Ni^{2+} cation mixing dominates the structural evolution of both $LiNiO_2$ and $LiNi_{0.8}Co_{0.2}O_2$, leading to the degradation of the layered structures and eventual complete phase transition back to rock-salt phase. In $LiNiO_2$, following severe degradation of the layered structure, the phase transition to rock salt is complete at 925 °C (Figure 1a and Figure S7); in contrast, the transition in $LiNi_{0.8}Co_{0.2}O_2$ is much delayed, to 975 °C (Figures 1b and 2b,d).

Throughout the process from Stage I to Stage III, the intermediates toward $LiNiO_2$ and $LiNi_{0.8}Co_{0.2}O_2$ undergo local structural ordering, and due to competition between lithiation of the Li-deficient layered phase and deterioration of cation ordering, a parabolic intensity change of (003) reflection occurs (Figure 1d). Manipulating the synthesis procedure can effectively balance the favorable lithiation process and unfavorable Ni^{2+} migration (along with Li/O loss), thereby optimizing the cationic ordering in the final layered product.

The results from refinements of ex situ synchrotron XRD data (as given in Table S3, Supporting Information) reveal the optimal compositions of $(Li^+{}_{0.9794}Ni^{2+}{}_{0.0206})_{3b}(Ni^{2+}{}_{0.0206}Ni^{3+}{}_{0.775}Co^{3+}{}_{0.204})_{3a}O_2$ and $(Li^+{}_{0.9647}Ni^{2+}{}_{0.0353})_{3b}(Ni^{2+}{}_{0.0353}Ni^{3+}{}_{0.9647})_{3a}O_2$, with and without Co substitution, respectively, which demonstrates the impact of Co substitution on restricting Li^+/Ni^{2+} cation mixing during the synthesis of Ni-rich layered oxides. The enhancement of cationic ordering with Co substitution may be explained by the size difference between Co^{3+} (0.55 Å) and Li^+ (0.76 Å), favoring the preoccupancy of Co^{3+} at 3a transition metal sites. Thus, the presence of Co^{3+} substituent, due to its similar ionic radius to Ni^{3+} (0.56 Å), would promote the formation of Li(Ni, Co)O_2 solid solution at low temperatures, eventually giving rise to cationic ordering within the layered structure.[13] Alternatively, the Co-substitution effects may be explained by the electronic configuration of the low-spin state of Co^{3+} ($t^6_{2g}e_g^0$): a stronger Ni^{3+}–O–Co^{3+} exchange interaction takes place within the transition metal layer of Li(NiCo)O_2 than in the transition metal layer of the $LiNiO_2$, and randomly distributed Co^{3+} ions in the transition metal layer of Li(NiCo)

O_2 screens the 180° Ni^{2+}–O–Ni^{2+} configurations, effectively reducing the Ni^{2+} population in Li layers.[3]

Therefore, Co-subsitution is crucial to cationic ordering in the solid solution $Li(NiCo)O_2$. But it should be noted that, high oxidation environment (i.e., in O_2 flow) is also important, particularly for suppressing Li/O loss during heat treatment at high temperatures, which was shown by the TGA analysis (Figure S1, Supporting Information) and has also been extensively demonstrated in the literatures.[11]

3.2. In Situ Synthetic Control of Structural/Electrochemical Properties of Layered Oxides

As illustrated in Figure 6, corresponding to the structural evolution of the intermediates (on the top panel), Li and Ni(Co) slab distances evolve with temperature (bottom panel), which may have important implications for synthetic control of the electrochemical properties of the electrode materials. For example, even a slight decrease in Li slab distance (i.e., 4%) may cause considerable increase in the activation energy for Li immigration (by more than 200%; or a few orders of magnitude reduction in Li diffusivity), as predicted by computational calculations.[25] Therefore, in order to meet the demands on high electrochemical activity of the layered oxides, control of the Li slab distance is needed and may be realized via fine-tuning of the synthesis conditions (temperature in particular). The plot suggests that $LiNi_{0.8}Co_{0.2}O_2$ should be synthesized at the temperature range 750–850 °C to maximize Li slab distance; in the materials synthesized at temperatures below or above the range, the slab distance is much reduced, suppressing Li diffusivity, and resulting in sluggish Li intercalation kinetics of the synthesized materials. Another relevant parameter is Ni(Co) slab distance, which, despite its much smaller effect on Li mobility,[26] is an important indicator of the oxidation state of Ni(Co) and relevant to the specific capacity and redox potential of the synthesized materials.

The information gained through these in situ studies, correlating synthesis conditions with Li and transition metal slab distances, may provide guidance for designing and synthesizing Ni-rich layered oxides, broadly in various NCM (i.e., Li–Ni–Co(Mn)–O) materials. As shown in Figure 5 and Figure S6 of the Supporting Information, high capacity (>200 mA h g^{-1}) may be achieved in $LiNi_{0.8}Co_{0.2}O_2$ cathodes by extending the range to high voltages, but with cycling stability sacrificed. The issue may be alleviated by Mn substitution, which, however, introduces equivalent Ni^{2+} into the layered structure, and so may induce the undesirable Li^+/Ni^{2+} cation mixing. So we expect that the approach developed here may be extended to studying the synthesis processes in preparing NCM cathodes, wherein the synthesis conditions have been found similarly vital to achieving high structural ordering and high capacity.[16]

4. Conclusion

Through in situ XRD studies of synthesis reactions in preparing $LiNiO_2$ and the Co-substituted variant, $LiNi_{0.8}Co_{0.2}O_2$, we obtained direct experimental evidence of direct transformation from rock salt to a Li-deficient layered phase, followed by a gradual structural ordering process during heat treatment. The results from studying the two contrasting systems, with and without Co substitution, show that the nature of the cation (i.e., ionic radius, size, valence state) may have significant impact on the structural evolution and phase transformation during synthesis of layered oxides. More specifically, Co substitution not only facilitates the initial nucleation of a Co-based layered phase at low temperatures, but also helps to stabilize the layered structure against Li and oxygen loss at high temperatures.

Guided by insights gained from in situ studies, we synthesized highly stoichiometric $LiNi_{0.8}Co_{0.2}O_2$ exhibiting high capacity (up to 200 mA h g^{-1}) and excellent retention. This work sheds light on the fundamental relationship between synthesis conditions and structural orderings of Ni-rich layered oxides, and may advance the design of synthetic protocols for making high-capacity Ni-rich layered oxide cathodes with stabilized structure and long cycling stability for next-generation lithium-ion batteries.

5. Experimental Section

Synthesis of Ni-Rich Layered $LiNiO_2$ and $LiNi_{0.8}Co_{0.2}O_2$: $Ni(CH_3COO)_2{\cdot}4H_2O$, $Co(CH_3COO)_2{\cdot}4H_2O$ and $CH_3COOLi{\cdot}2H_2O$ of certain molar ratios were dissolved into distilled (DI) water under magnetic stirring at 80 °C. The extra 3% of lithium source was used in order to compensate the volatilization of lithium at high heating temperatures. The resulted solution was continuously stirred to evaporate the solvent. Afterward, the mixture was dried in vacuum at 120 °C for 12 h. Heat treatments of the dried mixture were carried out either in the air for 20 h or in O_2 flow for 5 h at different temperatures with a ramp of 5 °C min^{-1}. The synthesized powders were collected after cooling to room temperature.

In Situ XRD Measurements: In situ XRD measurements of $LiNiO_2$ and $LiNi_{0.8}Co_{0.2}O_2$ were carried out under O_2 flow, using a Bruker D8 Advance Diffractometer equipped with an Anton Paar HTK 1200N high temperature attachment, Vantec-1 high speed PSD detector, and Cu anode X-ray tube. Similar procedures were used for measurements and data analysis as in a previous report.[27] The scanning rate was set to 2° min^{-1}, and the heating rate was 10 °C min^{-1}. The furnace chamber was flushed with flowing O_2 at 200 mL min^{-1} during all the measurements. Rietveld refinements of individual diffraction patterns were carried out using TOPAS 4.1 software to analyze concentration of the involved crystalline phases, Li^+ occupancy at 3b sites (Li sites), unit cell parameters (*a*, *c*), crystallite size and Ni–O and Li–O bond lengths of Ni-rich oxides as a function of heating temperature.

Synchrotron XRD Measurements: The ex situ synchrotron XRD measurements were performed at Beamline XPD (28-ID-2), National Synchrotron Light Source II, Brookhaven National Lab with a wavelength of 0.18045 Å. Rietveld refinements of XRD patterns were carried out using the TOPAS 4.1 software, based on the space group, $R\bar{3}m$, in which Li_1/Ni_2 was set at 3b site (0, 0, 0.5), $Li_2/\ Ni_1/Co_1/Mn_1$ at 3a site (0, 0, 0), and O at 6c site (0, 0, z) with $z \approx 0.25$.

NPD Measurements: Ex situ NPD data were collected on a set of selected samples at the POWGEN diffractometer located at the Spallation Neutron Source, Oak Ridge National Laboratory. A center wavelength of 1.333 Å was selected to cover a d-spacing range of 0.4–6 Å. Rietveld refinements of NPD patterns were carried out using the GSAS package with the EXPGUI interface.[28]

TEM-EELS Measurements: TEM-EELS measurements were performed on a JEOL 2100F microscope and a JEOL-ARM 200F microscope (with double C_s correctors and a cold-field emission gun), both operated at 200 kV. The powder sample dispersed on a TEM grid (with an amorphous carbon-membrane support) were loaded on to a TEM holder

and then transferred to the TEM column. TEM images and selected area electron diffraction (SAED) patterns were recorded by a charge-coupled device (CCD, Gatan).

Thermogravimetric Analysis (TGA) and Differential Thermal Analysis (DTA): TGA and DTA were performed on a SII STA7300 analyzer at a heating rate of 5 °C min^{-1} in air and O_2 flows, respectively.

Electrochemical Measurements: The electrodes were prepared by casting slurry of 80 wt% active materials, 10 wt% Super-P carbon, and 10 wt% poly-vinylidenefluoride (PVDF) as the binder on the Al foil. These cathodes were assembled into 2032-type coin cells in an argon-filled glove box for electrochemical measurements, with a metallic lithium foil (MTI Crop.) as the reference and counter electrode and glass microfiber (Whatman, GF/D) as the separator. The electrolyte was 1 M $LiPF_6$ dissolved in ethylene carbonate (EC) and dimethyl carbonate (DMC) at a volumetric ratio of 5:5 (BASF, USA). The galvanostatic charge-discharge performance was measured at different current densities using a battery cycler (Arbin Instrument, BT-2400) in constant current mode in different voltage ranges. Theoretical capacities of different cathode materials are all set to 200 mA h g^{-1} (i.e., the specific current corresponding to 1 *C* is 200 mA g^{-1}). Cyclic voltammetric (CV) curves of cathodes were recorded at a scanning rate of 0.1 mV s^{-1} in different voltage ranges.

Supporting Information

Supporting Information is available from the Wiley Online Library or from the author.

Acknowledgements

This work was supported by the U.S. Department of Energy (DOE) Office of Energy Efficiency and Renewable Energy under the Advanced Battery Materials Research (BMR) program under Contract No. DE-SC0012704. Laboratory in situ XRD measurements carried out at Alfred University (X-ray Diffraction and Scatting Lab) were supported by the Inamori Professorship held by SM. Synchrotron X-ray and TEM-EELS measurements carried out at the Center for Functional Nanomaterials and the National Synchrotron Light Source II (XPD beamline; 28-ID-2), Brookhaven National Laboratory, were supported by the U.S. Department of Energy, Office of Basic Energy Sciences, under Contract No. DE-SC0012704. Neutron powder diffreaction measurement at ORNL's Spallation Neutron Source was sponsored by the Scientific User Facilities Division, Office of Basic Energy Sciences, U.S. Department of Energy. L.W. and Y.Z. were supported by the U.S. Department of Energy, Office of Basic Energy Science, Division of Materials Science and Engineering under Contract No. DE-SC0012704. We thank John Johnson, Yusuf Celebi, Eric Dooryhee, Sanjit Ghose and John Trunk for technical support. We thank Dawei Wang, Patrick Looney, Gerbrand Ceder and Wei Tong for insightful discussions.

Received: June 13, 2016
Revised: August 24, 2016
Published online:

[1] a) C. R. Brown, E. McCalla, C. Watson, J. R. Dahn, *ACS Comb. Sci.* **2015**, *17*, 381; b) M. S. Whittingham, *Chem. Rev.* **2014**, *114*, 11414; c) A. Manthiram, J. C. Knight, S.-T. Myung, S.-M Oh, Y.-K. Sun, *Adv. Energy Mater.* **2016**, *6*, 1501010; d) P. Rozier, J. M. Tarascon, *J. Electrochem. Soc.* **2015**, *162*, A2490; e) J. B. Goodenough, Y. Kim, *Chem. Mater.* **2010**, *22*, 587.

[2] a) D.-W. Seo, J. Lee, A. Urban, R. Malik, S. Y. Kang, G. Ceder, *Nat. Chem.* **2016**, *4*, 1400478; b) A. Urban, J. Lee, G. Ceder, *Adv. Energy Mater.* **2014**, *8*, 692; c) M. Gu, I. Belharouak, J. Zheng, H. Wu, J. Xiao, A. Genc, K. Amine, S. Thevuthasan, D. R. Bae, J-g. Zhang, N. D. Brown, J. Liu, C. Wang. *ACS Nano* **2012**, *7*, 760; d) Y.-K. Sun, Z. Chen, H.-J. Noh, D.-J. Lee, H.-G. Jung, Y. Ren, S. Wang, C. S. Yoon, S.-T. Myung, K. Amine, *Nat. Mater.* **2012**, *11*, 942; e) F. Lin, I. M. Markus, D. Nordlund, T.-C. Weng, M. D. Asta, H. L. Xin, M. M. Doeff, *Nat. Commun.* **2014**, *5*, 3529; f) B. R. Long, J. R. Croy, F. Dogan, M. R. Suchomel, B. Key, J. Wen, D. J. Miller, M. M. Thackeray, M. Balasubramanian, *Chem. Mater.* **2014**, *26*, 3565; g) G. Cherkashinin, D. Ensling, W. Jaegermann, *J. Mater. Chem. A* **2014**, *2*, 3571; h) X. Li, F. Cheng, B. Guo, J. Chen, *J. Phys. Chem. B* **2005**, *109*, 14017; i) G. Xu, Z. Liu, C. Zhang, G. Cui, L. Chen, *J. Mater. Chem. A* **2015**, *3*, 4092; j) F. Lin, N. Dennis, L. Yuyi, K. Q. Matthew, C. Lei, T.-C. Weng, Y. Liu, H. L. Xin, M. M. Doeff, *Nat. Energy* **2016**, *1*, 15004.

[3] a) W. Liu, P. Oh, X. Liu, M.-J. Lee, W. Cho, S. Chae, Y. Kim, J. Cho, *Angew. Chem. Int. Ed.* **2015**, *54*, 4440; b) S. Hwang, D. H. Kim, K. Y. Chung, W. Chang, *App. Phys. Lett.* **2014**, *105*, 103901; c) J.-Y. Liao, A. Manthiram, *J. Power Sources* **2015**, *282*, 429; d) H. Kim, M. G. Kim, H. Y. Jeong, H. Nam, J. Cho, *Nano Lett.* **2015**, *15*, 2111; e) I. Hwang, C. W. Lee, J. C. Kim, S. Yoon, *Mater. Res. Bull.* **2012**, *47*, 73; f) F. Wu, J. Tian, Y. Su, J. Wang, C. Zhang, L. Bao, T. He, J. Li, S. Chen, *ACS App. Mater. Interfaces* **2015**, *7*, 7702; g) C. Fu, G. Li, D. Luo, Q. Li, J. Fan, L. Li, *ACS App. Mater. Interfaces* **2014**, *6*, 15822; h) L. Wu, K.-W. Nam, X. Wang, Y. Zhou, J.-C. Zheng, X.-Q. Yang, Y. Zhu, *Chem. Mater.* **2011**, *23*, 3953; i) H. Chen, J. A. Dawson, J. H. Harding, *J. Mater. Chem. A* **2014**, *2*, 7988; i) H. Chen, J. A. Dawson, J. H. Harding, *J. Mater. Chem. A* **2014**, *2*, 7988; j) A. Manthiram, J. C. Knight, S.-T. Myung, S.-M. Oh, Y.-K. Sun, *Adv. Energy Mater.* **2015**, *6*, 1501010; k) M. Jo, M. Noh, P. Oh, Y. Kim, J. Cho, *Adv. Energy Mater.* **2014**, *4*, 1301583.

[4] a) A. Rougier, I. Saadoune, P. Gravereau, P. Willmann, C. Delmas, *Solid State Ionics* **1996**, *90*, 83; b) P. Kalyani, N. Kalaiselvi, *Sci. Technol. Adv. Mater.* **2005**, *6*, 689; c) H. H. Li, N. Yabuuchi, Y. S. Meng, S. Kumar, J. Breger, C. P. Grey, Y. Shao-Horn, *Chem. Mater.* **2007**, *19*, 2551.

[5] P. Yan, J. Zheng, D. Lv, Y. Wei, J. Zheng, Z. Wang, S. Kuppan, J. Yu, L. Luo, D. Edwards, M. Olszta, K. Amine, J. Liu, J. Xiao, F. Pan, G. Chen, J.-G. Zhang, C.-M. Wang, *Chem. Mater.* **2015**, *27*, 5393.

[6] Y. Wei, J. Zheng, S. Cui, X. Song, Y. Su, W. Deng, Z. Wu, X. Wang, W. Wang, M. Rao, Y. Lin, C. Wang, K. Amine, F. Pan, *J. Am. Chem. Soc.* **2015**, *137*, 8364; b) C. Delmas, M. Ménétrier, L. Croguennec, I. Saadoune, A. Rougier, C. Pouillerie, G. Prado, M. Grüne, L. Fournès, *Electrochim. Acta* **1999**, *45*, 243.

[7] a) Y. K. Sun, D. J. Lee, Y. J. Lee, Z. Chen, S. T. Myung, *ACS App. Mater. Interfaces* **2013**, *5*, 11434; b) J. Zheng, W. H. Kan, A. Manthiram, *ACS App. Mater. Interfaces* **2015**, *7*, 6926; c) D. Kim, J. M. Lim, Y. G. Lim, J. S. Yu, M. S. Park, M. Cho, K. Cho, *Chem. Mater.* **2015**, *27*, 6450.

[8] S.-P. Lin, K.-Z. Fung, Y.-M. Hon, M.-H. Hon, *J. Solid State Chem.* **2002**, *167*, 97.

[9] a) Y. H. Jouybari, S. Asgari, *J. Power Sources* **2011**, *196*, 337; b) H. Liu, Z. Zhang, Z. Gong, Y. Yang, *Solid State Ionics* **2004**, *166*, 317; c) X. Cao, L. Xie, R. Wang, *J. Solid State Electrochem.* **2011**, *15*, 473.

[10] a) R. K. B. Gover, R. Kanno, B. J. Mitchell, M. Yonemura, Y. Kawamoto, *J. Electrochem. Soc.* **2000**, *147*, 4045; b) J.-H. Shim, C.-Y. Kim, S.-W. Cho, A. Missiul, J.-K. Kim, Y. J. Ahn, S. Lee, *Electrochim. Acta* **2014**, *138*, 15; c) D. Jiang, L. Zhao, Y. Shao, D. Wang, *RSC Adv.* **2015**, *5*, 40779; d) Y. Bi, W. Yang, R. Du, J. Zhou, M. Liu, Y. Liu, D. Wang, *J. Power Sources* **2015**, *283*, 211.

[11] a) S. P. Lin, K. Z. Fung, Y. M. Hon, M. H. Hon, *J. Cryst. Growth* **2001**, *226*, 148; b) M. Sobri Idris, A. R. West, *J. Electrochem. Soc.* **2012**, *159*, A396; c) S.-W. Lee, H. Kim, M.-S. Kim, H.-C. Youn, K. Kang, B.-W. Cho, K. C. Roh, K.-B. Kim, *J. Power Sources* **2016**, *315*, 261.

[12] H. Yu, Y. Qian, M. Otani, D. Tang, S. Guo, Y. Zhu, H. Zhou, *Energy Environ. Sci.* **2014**, *7*, 1068.

[13] P. Rozier, J. M. Tarascon, *J. Electrochem. Soc.* **2015**, *162*, A2490.
[14] S.-P. Lin, K.-Z. Fung, Y.-M. Hon, M.-H. Hon, *J. Cer. Soc. Jpn.* **2002**, *110*, 1038.
[15] B. V. L'vov, *Thermochim. Acta* **2000**, *360*, 109.
[16] Y. Li, R. Xu, Y. Ren, J. Lu, H. Wu, L. Wang, D. J. Miller, Y.-K. Sun, K. Amine, Z. Chen, *Nano Energy* **2015**, *19*, 522.
[17] R. K. B. Gover, R. Kanno, B. J. Mitchell, A. Hirano, Y. Kawamoto, *J. Power Sources* **2000**, *97*, 316.
[18] Y. Koyama, T. Mizoguchi, H. Ikeno, I. Tanaka, *J. Phys. Chem. B* **2005**, *109*, 10749.
[19] a) M. Gu, I. Belharouak, A. Genc, Z. Wang, D. Wang, K. Amine, F. Gao, G. Zhou, S. Thevuthasan, D. R. Baer, J.-G. Zhang, N. D. Browning, J. Liu, C. Wang, *Nano Lett.* **2012**, *12*, 5186; b) A. Boulineau, L. Simonin, J. F. Colin, C. Bourbon, S. Patoux, *Nano Lett.* **2013**, *13*, 3857.
[20] W. Li, J. N. Reimers, J. R. Dahn, *Solid State Ionics* **1993**, *67*, 123.
[21] I. Saadoune, C. Delmas, *J. Solid State Chem.* **1998**, *136*, 8.
[22] E. Levi, M. D. Levi, G. Salitra, D. Aurbach, R. Oesten, U. Heider, L. Heider, *Solid State Ionics* **1999**, *126*, 97.
[23] X. Zhang, W. J. Jiang, A. Mauger, Qilu, F. Gendron, C. M. Julien, *J. Power Sources* **2010**, *195*, 1292.
[24] a) J. Xu, F. Lin, D. Nordlund, E. J. Crumlin, F. Wang, J. Bai, M. M. Doeff, W. Tong, *Chem. Commun.* **2016**, *52*, 4239; b) Z. Chen, J. Wang, D. Chao, T. Baikie, L. Bai, S. Chen, Y. Zhao, T. C. Sum, J. Lin, Z. Shen, *Sci. Rep.* **2016**, *6*, 25771.
[25] Y. Kan, Y. Hu, Y. Ren, J. Bareño, I. Bloom, Y.-K. Sun, K. Amine, Z. Chen, *J. Power Sources* **2014**, *271*, 97.
[26] K. Kang, G. Ceder, *Phys. Rev. B* **2006**, *74*, 094105.
[27] L. Wang, J. Bai, P. Gao, X. Wang, J. P. Looney, F. Wang, *Chem. Mater.* **2015**, *27*, 5712.
[28] a) A. C. Larson, R. B. V. Dreele, "*General Structure Analysis System (GSAS)", Los Alamos Natl. Lab., [Rep.] LA (U.S.)* **1994**, LAUR 86-748; b) B. H. Toby, *J. Appl. Crystallogr.* **2001**, *34*, 210.